

Preparation of reduced graphene oxide supported palladium nanocomposites for amperometric sensing of NADH

Xuyan Mao^{1,*}, Xiaomeng Wang², Xiangyu Xu³, Liang Jiang¹, Jie Yang¹, Zhongyu Du³,
Qingsheng Kong^{1,*}

¹ Collaborat Innovat Ctr Birth Defect Res & Transfo, Jining Medical University, Jining, 272067, Shandong, China.

² College of Health, Yantai Nanshan University, Yantai, 265713, Shandong, China.

³ College of Basic Medicine, Jining Medical University, Jining, 272067, Shandong, China.

*E-mail: xuyanm_06@163.com, jnyxykqs@163.com

Received: 14 January 2020 / Accepted: 14 April 2020 / Published: 10 June 2020

Reduced graphene oxide-supported palladium nanocomposites (Pd-rGO) were synthesized by an in situ chemical reduction method. The composite nanomaterials have excellent conductivity and catalytic ability due to the synergistic effect of the two components. Experiments show that Pd-rGO has a prominent advantage in electrochemical catalysis for NADH. The oxidation potential of NADH at the Pd-rGO/GCE is negatively shifted by 0.6 V relative to that at the rGO/GCE. The measurement of NADH can be obtained with a high sensitivity of $110 \text{ nA} \cdot \mu\text{M}^{-1} \cdot \text{cm}^{-2}$ under the low potential of 0.0 V, with minimal interference. The concentration range of NADH was between 0.31 μM and 350 μM , with a detection limit (S/N = 3) of 93 nM.

Keywords: Reduced graphene oxide, Palladium nanoparticles, Electrocatalysis, NADH

1. INTRODUCTION

Dihyronicotinamide adenine dinucleotide (NADH) and its oxidized form (NAD⁺) are responsible for the catalytic reactions of all NAD(H)-dependent enzymes[1]. The electrochemical oxidation of NADH is very significant in the construction of electrochemical biosensors, and the effective recovery of NADH/NAD⁺ is necessary. NAD⁺ reduction and NADH oxidation show obvious irreversibility on solid electrodes, with overpotentials up to 1 V. These issues lead to serious interference in the presence of simultaneously existing electroactive substances such as ascorbic acid and uric acid. Moreover, a high overpotential easily leads to the formation of inactive dimers, thus contaminating the electrode surface[5]. In the past few years, many methods have been tested to

decrease the oxidation overpotential of NADH on electrodes either directly or by using a suitable medium.

In recent years, with the continuous development of nanomaterials, a variety of biosensors have emerged made from carbon-based nanomaterials, such as mesoporous carbon [2] and carbon nanotubes [3]. With the in-depth study of the structure and properties of graphene, its application in electrochemistry, especially in the field of bioelectrochemistry, has attracted increasing attention [4-11]. Graphene is an ideal electrode material for electrochemical biosensors because of its excellent conductivity and electrocatalytic performance [12-13]. The good electrical properties of graphene make it possible to effectively promote electron transport during the electrochemical process, improve the sensitivity and response signal of biosensors, and shorten the response time [14]. Moreover, graphene has a large specific surface area that can effectively increase the loading of active materials, thereby improving the sensitivity and other properties of the sensor [15]. In addition, graphene has good biocompatibility to maintain biological activity and is conducive to the stability of biosensors [16,17]. The monoatomic thickness and two-dimensional planar structure of graphene provide a large specific surface area, which can be used to load a large number of compounds, including metals, biological molecules and a variety of drugs. Therefore, graphene has many potential applications in the detection of bioactive substances, especially in biosensor technology. Many research results show that graphene as a support material and biological platform can effectively improve the performance of biosensors. Graphene is oxidized to produce abundant oxygen-containing functional groups on the surface, but at the same time, this process destroys its π -conjugated system, which has a great impact on its electronic, mechanical and electrochemical properties. Compared with graphene oxide (GO), reduced graphene oxide (rGO) has better conductivity. Studies have shown that electrodes modified by rGO exhibit a better electrochemical response to some bioactive molecules.

Metals and their oxides have excellent conductivity and catalytic performance, so they can enhance the electron transfer performance and improve the electrochemical reaction rate of graphene-based modified electrodes. Some metals and their oxides are loaded on the graphene surface by chemical reduction, physical adsorption and electrochemical deposition methods, such as gold, platinum, palladium, Fe_3O_4 , CoO_2 , TiO_2 and ZnO nanoparticles [18-22]. Yanyan Zhang et al. fabricated a novel and efficient enzyme-free hydrogen peroxide sensor by modifying the electrode with PVP, graphene and palladium nanoparticle composite materials. The composite materials showed high electrocatalytic activity for the reduction of H_2O_2 and achieved rapid direct electron transfer [18]. Tian filled titanium dioxide nanotube arrays (TiO_2 NTs) with graphene quantum dots and applied the composite as an efficient ECL emitter for biosensing of prostate serum antigen (PSA). Such an immunosensor was applied to measure PSA in clinical human serum samples of prostate cancer patients and controls with excellent correlation to the referee chemiluminescence method [20].

In this work, using an in situ synthesis method, reduced graphene oxide (rGO) was functionalized with palladium nanoparticles, which have high conductivity and good electrocatalytic performance. The nanocomposites have prominent advantages in electrochemical catalysis for NADH, such as greatly reduced overpotential as well as high sensitivity and selectivity.

2. EXPERIMENTAL SECTION

2.1. Reagents

A graphene oxide (GO) dispersion in water was obtained from Jining LeaderNano Company; palladium chloride and sodium borohydride (NaBH_4) were obtained from Alfa Aesar (China); and β -nicotinamide adenine dinucleotide, reduced disodium salt hydrate (NADH), ascorbic acid (AA), acetaminophen (AP), dopamine (DA) and uric acid (UA) were obtained from Sigma-Aldrich. All other chemicals were analytical grade and used as obtained, and the aqueous solutions were made of ultrapure water.

2.2. Instrumentation

Electrochemical measurements were carried out on a CHI 660E electrochemical workstation (Shanghai Chenhua Instrument Co., Ltd., China). The electrochemical cell was assembled as a traditional three electrode system. A coiled platinum wire was used as the counter electrode. A modified glassy carbon (GC) electrode was used as the working electrode. All potentials refer to the sodium saturated calomel electrode (SSCE). All electrochemical tests were performed at room temperature (approximately 25 °C).

2.3. Procedures

2.3.1. Preparation of Pd-rGO and rGO nanomaterials

The synthetic methods of nanomaterials were performed according to a previously reported article [23]. First, 77 ml of GO dispersion (1.3 mg ml^{-1}) was used as obtained and sonicated for 10 minutes to obtain a homogeneous dispersion. Then, 8.8 mg of PdCl_2 was dissolved in 5 ml of ultrapure water and acidified with 7.2 μl of conc. HCl. The above solutions were added to the GO dispersions, followed by sonication for 30 minutes. Reduction started when 72.44 mg of NaBH_4 freshly dissolved in 2.0 ml of ultrapure water was added to the slurry, and the reaction was cooled in an ice bath and magnetically stirred. After 5 min, cooling was stopped, and the mixture was stirred at room temperature for another 4 h. Next, Pd-rGO nanocomposite solid powder was obtained by centrifugation for 5 minutes at 10000 rpm, washed with ultrapure water and methanol three times and dried for 12 hours at 50 °C in a vacuum desiccator. The rGO nanomaterials were prepared as described above, while PdCl_2 was not added. Then, 2.0 mg of the solid nanomaterials was dispersed in 2.0 ml of ultrapure water and stirred by ultrasonication for 1 hour to obtain a well-dispersed suspension for modification of the working electrode.

2.3.2. Preparation of Pd-rGO/GC and rGO/GC electrodes

The glassy carbon electrode (GC, 3 mm diameter, CHI 104) was successively polished with alumina slurries of 1.0 μm , 0.3 μm and 0.05 μm , thoroughly cleaned with ultrapure water between the

polishing steps, cleaned by ultrasonication in ethanol and deionized water and finally dried in air. Then, 5 μl of the Pd-rGO or rGO suspension (1.0 mg ml^{-1} in water) was cast onto the surface of the pretreated GC electrode (denoted as Pd-rGO/GC or rGO/GC) with a microsyringe, and the solvent was dried at ambient temperature before use.

3. RESULTS AND DISCUSSION

3.1. Characterization of the Pd-rGO nanomaterials

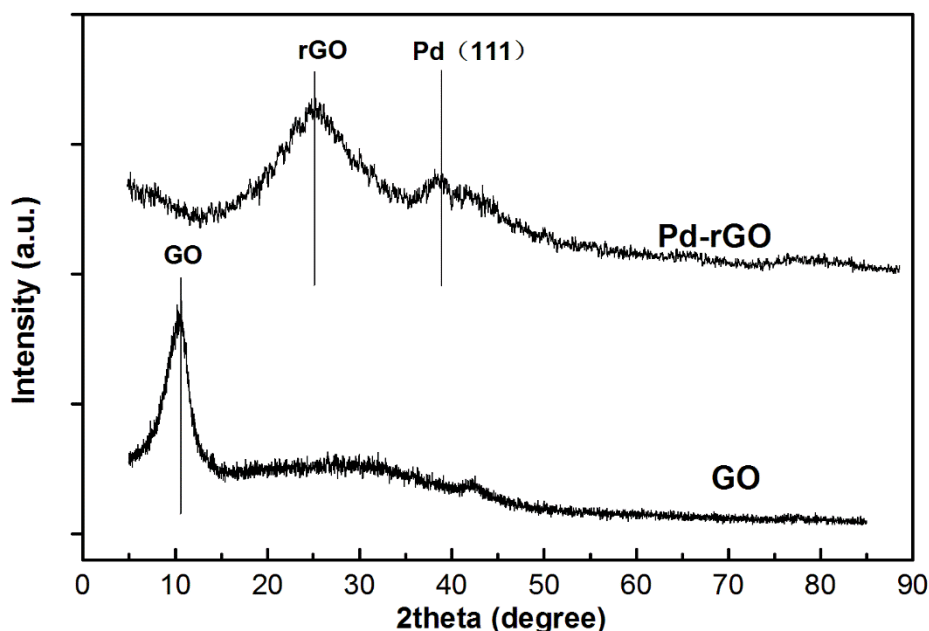


Figure 1. XRD patterns of the Pd-rGO and GO nanomaterials.

Fig. 1 shows the XRD patterns of the GO and Pd-rGO nanomaterials. The reflections characteristic of GO are at $2\Theta \approx 10.6^\circ$, while the reflection at $2\Theta \approx 25.4^\circ$ is from the graphene (002) plane[24]. The diffraction peak of the GO reflection at $2\Theta \approx 10.6^\circ$ disappears in the composite nanomaterials, indicating that the GO has been completely reduced to rGO. The reflection exhibited at $2\Theta \approx 40.1^\circ$ is from the Pd (111) plane[23], which suggests that Pd nanoparticles were successfully loaded onto rGO.

The topography and height profiles of GO and Pd-rGO measured with SPM are presented in Fig. 2. The thickness of the GO sheets was established to be 1.05 nm (from Fig. 2A), which corresponds to a single-layer graphene oxide. The B-line of Fig. 2a shows that the single-layer graphene sheet is folded so that the height becomes 1.98 nm. From Fig. 2b, we can see that the Pd nanoparticles were uniformly loaded on the rGO sheets, and the height of Pd-rGO was defined to be in the range of 6-8 nm. The height of the Pd nanoparticles is approximately 5-7 nm after removing the thickness of graphene.

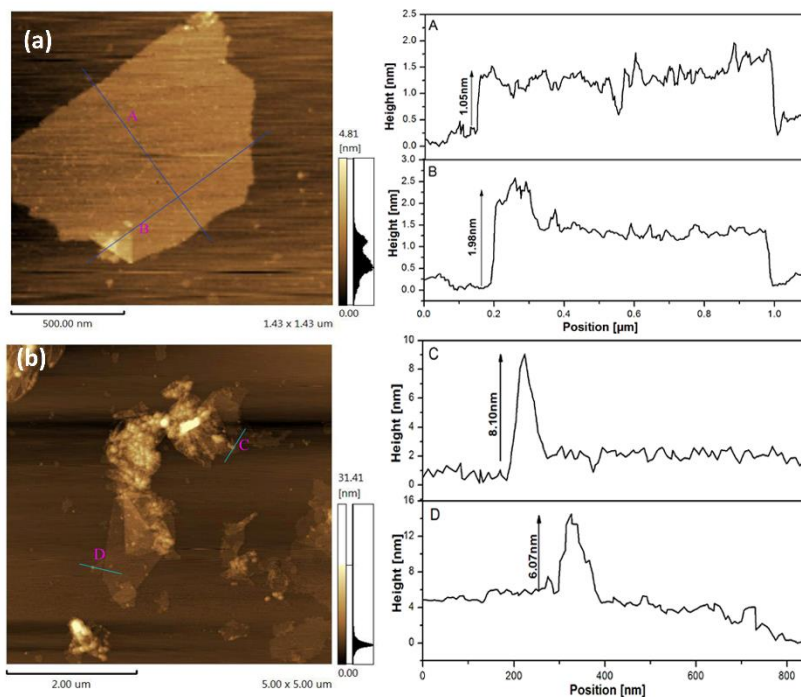


Figure 2. SPM image of GO(a) and Pd-rGO(b) and the height profile.

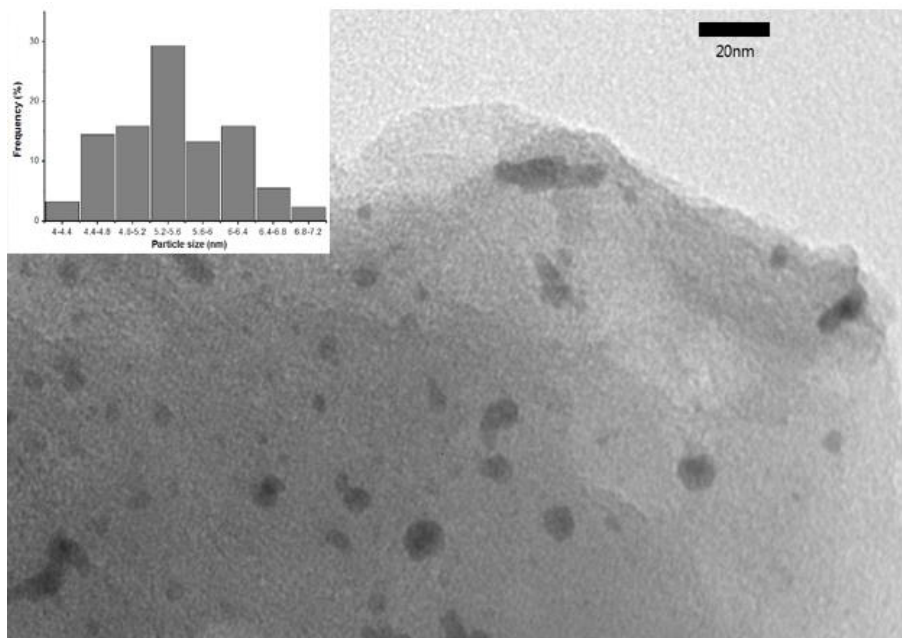


Figure 3. TEM images of Pd-rGO and particle size distributions are shown as insets.

The morphology and structure of the Pd-rGO was observed by TEM analysis. Fig. 3 shows the typical 2D wrinkled and crumpled structure of the reduced graphene oxide sheets with uniformly distributed palladium nanoparticles. The surface is densely packed with Pd nanoparticles, and no individual rGO sheets are observed. The average diameter of the Pd nanoparticles was 5.61 nm, as shown in the inset figure. This result is basically consistent with the thickness of the Pd-rGO

nanomaterial measured by SPM. The particle size of Pd is slightly larger than that in reference[23].

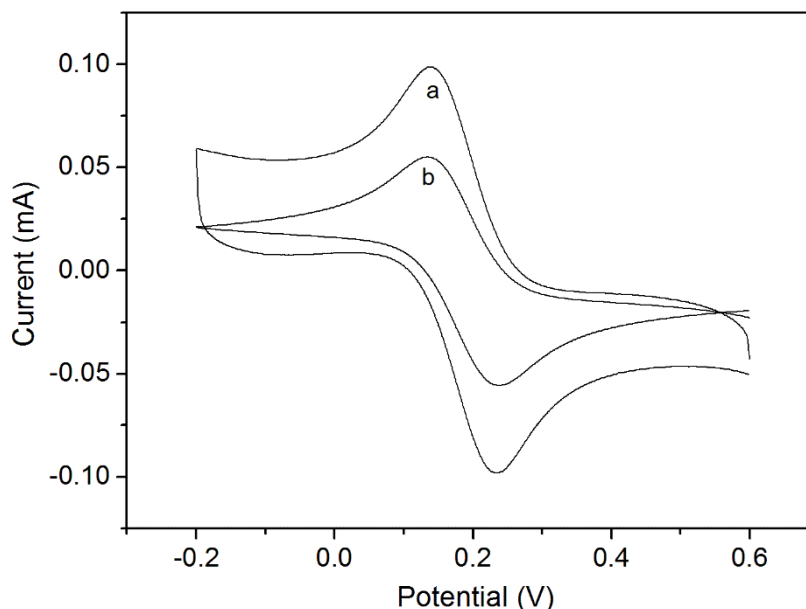


Figure 4. The cyclic voltammetry (CV) responses of the rGO/GCE (a) and Pd-rGO/GCE (b) achieved in a 50 mM potassium ferricyanide solution in 0.05 mol L⁻¹ pH 7.0 PBS. Scan rate, 50 mV s⁻¹.

3.2. Electrochemical characterization of Pd-rGO/GCE

To assess the electrochemical reactivity of the Pd-rGO-modified GCE (Pd-rGO/GCE), cyclic voltammetry (CV) was performed. Fig. 4 depicts the cyclic voltammetry curves for the rGO/GCE (a) and Pd-rGO/GCE (b) in a 50 mM potassium ferricyanide solution at a scan rate of 50 mV s⁻¹. A pair of well-defined and symmetric waves were obtained at both electrodes. Compared to rGO, Pd-rGO shows better electrochemical responses in the peak current (I_p) and peak separation (ΔE_p). The peak currents of Pd-rGO/GCE are much larger than those of rGO/GC, which is mainly due to the electroactivity of Pd nanoparticles on the graphene nanosheets. The peak separation was 94 mV and 104 mV for Pd-rGO/GCE and rGO/GCE, respectively. The former was much lower, revealing the facilitated electron transfer of [Fe(CN)₆]⁴⁻/[Fe(CN)₆]³⁻ at the Pd-rGO/GC electrode.

3.3. Electrocatalytic oxidation of NADH

To test the potential electrocatalytic activities of the Pd-rGO nanocomposite, cyclic voltammetric responses were recorded at Pd-rGO/GC and rGO/GC electrodes in the absence and presence of NADH. As shown in Fig. 5A, upon the addition of 1.0 mM NADH, the anodic peak currents increase, accompanied by decreased cathodic peak currents at the Pd-rGO/GCE, and the anodic peak potential is approximately 0.0 V. There is just an increased anodic peak current at the rGO/GC electrodes, with a peak potential of approximately 0.6 V, which is more positive than that of the Pd-rGO/GCE. This result is in agreement with other previous reports [25] In addition, at 0.0 V, the anodic current for NADH electroreoxidation at the Pd-rGO/GCE is much higher than that at the

rGO/GCE. These results suggest that compared to the rGO/GCE, the Pd-rGO/GCE possesses much higher electrocatalytic activity towards NADH. All the results above indicate the high possibility of using the Pd-rGO/GCE for NADH detection with high selectivity and sensitivity.

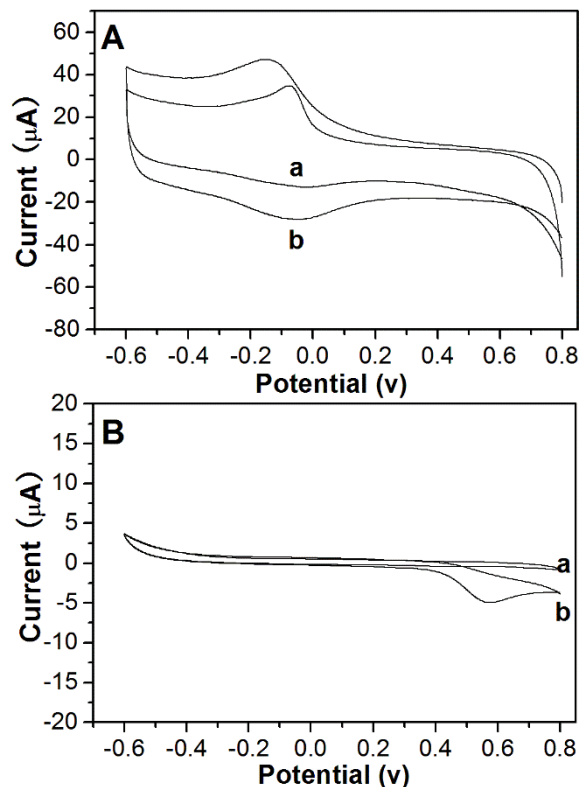


Figure 5. Cyclic voltammograms at the Pd-rGO/GCE (A) and rGO/GCE (B) recorded in phosphate buffer (pH 7.0, 0.05 mol L⁻¹) in the absence (a) and presence of 1.0 mM (b) NADH. Scan rate, 50 mV s⁻¹.

3.4. Interference detection of the Pd-rGO/GCE

The catalytic potential of the Pd-rGO/GCE for NADH is approximately 0.0 V. To verify whether some biological substances can interfere with the detection of NADH at this potential, we added 1.0 mM NADH to a continuously stirred phosphate buffer solution (pH 7.0, 0.05 M) at a potential of 0.0 V. After the response current was stabilized, 0.1 mM DA, 0.1 mM UA, and 0.1 mM AA were sequentially added. As shown in Fig. 6, DA and UA have almost no effect on the electrode response current, while AA shows less interference with the assay.

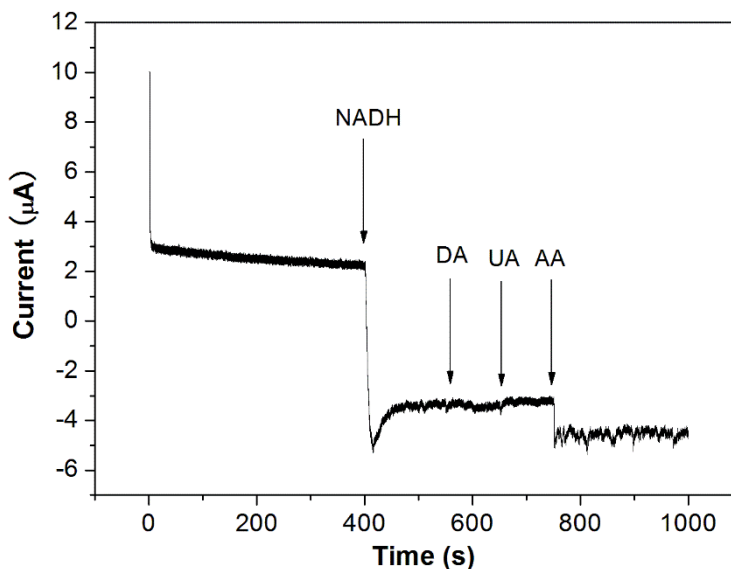


Figure 6. Amperometric response of the Pd-rGO/GCE in phosphate buffer solutions (pH 7.0, 0.05 mol L⁻¹) containing 1.0 mM NADH spiked with DA (0.10 mM), UA (0.10 mM) and AA (0.10 mM).

3.5. Electrochemical detection of NADH using the Pd-rGO/GCE

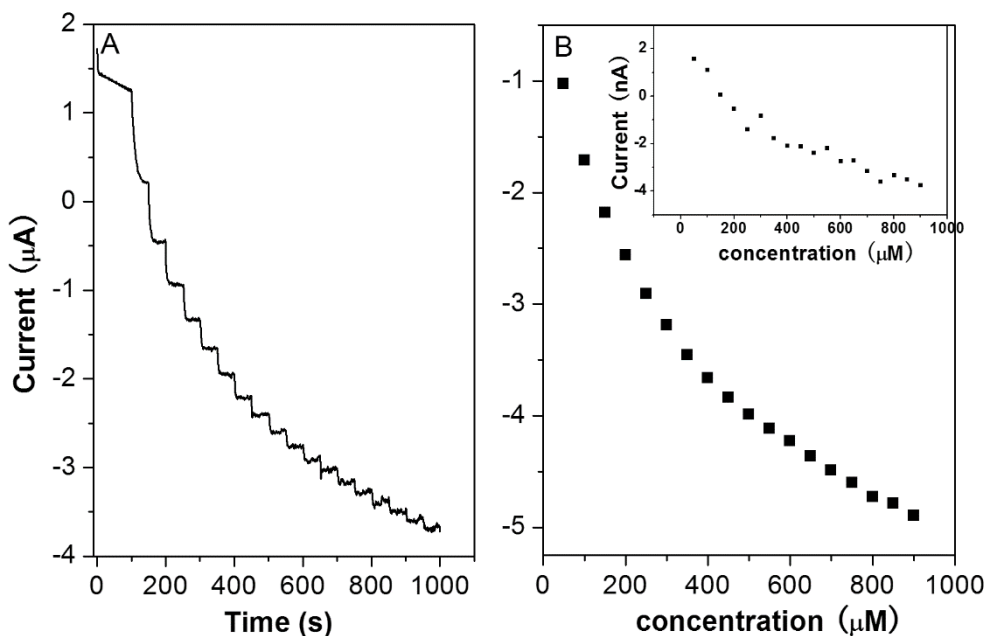


Figure 7. (A) Current-time responses for the rGO/pd/GCE with successive addition of 50 μM NADH. (B) Calibration curves for NADH at the Pd-rGO/GCE and rGO/GCE (insert curve). Phosphate buffer solutions: pH 7.0, 0.05 M; Operating potential: 0.0 V.

Table 1. The statistical data for NADH determination at the two modified electrodes.

Modified Electrode	E_{app} (mV)	Linear range (μM)	Detection limit (μM)	Sensitivity ($\text{nA}\cdot\mu\text{M}^{-1}\cdot\text{cm}^{-2}$)	Response time (s)
Pd-rGO/GCE	0.0	0.31–350	0.093	110	5
rGO/GCE	0.0	2.23 – 250	0.668	0.214 ²	20

Fig. 7 shows the current-time response of the Pd-rGO/GCE and rGO/GCE at a working potential of 0.0 V. A concentration of 50 μM NADH was continuously added dropwise to a phosphate buffer solution (pH 7.0, 0.05 M) at intervals of 50 s. The response times of the Pd-rGO/GCE and rGO/GCE were approximately 5 s and 20 s, respectively. After each sample solution was added, the reaction at the Pd-rGO/GCE reached dynamic equilibrium very quickly, and a steady-state current signal was generated within 4 s instead of 10 s at the rGO/GCE. The B diagram is a corresponding concentration-current standard curve. According to the standard curve, the electrode parameters of the corresponding electrode can be calculated. The detection limit, based on a signal-to-noise ratio of 3, is calculated as 0.093 μM , the linear range is from 0.31 μM to 350 μM , and the sensitivity is 110 $\text{nA}\cdot\mu\text{M}^{-1}\cdot\text{cm}^{-2}$. Under the same experimental conditions, the linear relationship of NADH catalysed by the rGO/GCE is studied. When the potential is as low as 0.0 V, the response current of the rGO/GCE to NADH is very small, and the linear range is very narrow. The detection limit was calculated as 0.668 μM , the linear range was from 2.23 μM to 250 μM , and the sensitivity was 0.214 $\text{nA}\cdot\mu\text{M}^{-1}\cdot\text{cm}^{-2}$. Table 1 lists the statistical data for NADH determination at the two modified electrodes. After comparison, it is observed that the Pd-rGO/GCE has a lower detection limit of NADH than the rGO/GCE, with a wider linear range and higher sensitivity. Table 2 summarizes the electrical analysis characteristics of some reported NADH sensors and compares them with those obtained in this study. The results showed that the sensitivity, linear range and detection limit of the Pd-rGO/GCE were significantly better than those of other nanocomposite electrodes. The synergistic effect of Pd and rGO on NADH oxidation improves the sensitivity and detection limit of the sensor.

Table 2. Comparison of the parameters of similar NADH sensors.

Modified Electrode	E_{app} (V)	Linear range (μM)	Detection limit (μM)	Sensitivity	Refs.
CNT-chitosan/GCE	+0.4	5–300	3 μM	130 $\text{mA}\cdot\text{M}^{-1}\cdot\text{cm}^{-2}$	[26]
NB/OMC/GCE	-0.1	–350	1.3 μM	648 nA/mM	[27]
PdNPs-MWCNTs/GCE	+0.45	0.1–200	0.032 μM	423 $\text{nA}\cdot\mu\text{M}^{-1}\cdot\text{cm}^{-2}$	[28]
Au-RGO/Chit/GCE	+0.35	1.5–320	1.2 μM	12 $\text{nA}\cdot\mu\text{M}^{-1}\cdot\text{cm}^{-2}$	[29]
B-CNDs/GCE	--	5.0–100	0.92	--	[30]

SPCE/RGO/PNR/Au NP	+0.15	100-2500	0.72	10.72 $\mu\text{A mM}^{-1}$	[31]
GC/CNTs/TTF/HRP	-0.3	10-790	1.53	--	[32]
TCBQ-LCPs/SWCNTs	+0.13	5-1650	0.82	4.99 $\mu\text{A mM}^{-1}$	[33]
Pd-rGO/GCE	0.0	0.31-350	0.093 μM	110 $\text{nA} \cdot \mu\text{M}^{-1} \cdot \text{cm}^{-2}$	This work

The operational stability of the NADH sensor was studied under continuous use for 10 h. The current response decreased by only approximately 9% within 10 h, which indicated that the Pd-rGO/GCE has good operational stability and can be used continuously for several hours. We measured the reproducibility of the assay by repeating the method five times, and the value of the relative standard deviation (RSD%) was approximately 6.5%.

4. CONCLUSIONS

We demonstrate reduced graphene oxide-supported palladium (Pd-rGO) nanocomposites prepared by an in situ chemical reduction method. The structure of the Pd-rGO nanocomposites was identified by XRD and characterized by SPM and TEM. It was found that the Pd nanoparticles in the composite were uniformly loaded on the rGO sheets. The Pd-rGO nanocomposite has a prominent advantage in electrochemical catalysis for NADH. In view of our results, we successfully designed a NADH sensor with low potential as well as high sensitivity and selectivity.

ACKNOWLEDGEMENTS

The authors are profoundly grateful for the financial support provided by Natural Science Foundation of Shandong Province (Nos. ZR2019PB026, ZR2017BB015, and ZR2018PB011) and NSFC cultivation project of Jining Medical University (Nos. JYP20418KJ17 and JYP2018KJ03).

References

1. L. Gorton, P.N. Bartlett, John Wiley & Sons, Ltd, 2008, 157.
2. M. Zhou, J. Guo, L. Guo and J. Bai, *Anal. Chem.*, 80 (2008) 4642.
3. M. Wooten and W. Gorski, *Anal. Chem.*, 82(2010) 1299.
4. D. Chen , H. Feng and J. Li, *Chem. Rev.*, 112 (2012) 6027.
5. D. Chen, L. Tang and J. Li, *Chem. Soc. Rev.*, 39(2010) 3157.
6. L. Tang , Y. Wang, Y. Liu and J. Li, *ACS Nano*, 5 (2011) 3817.
7. M. Pumera, A. Ambrosi, A. Bonanni, E. L. Khim Chng and H. L. Poh, *Trac-Trend Anal. Chem.*, 29 (2010) 954.
8. S. Kochmann, T. Hirsch and O. S. Wolfbeis, *Trac-Trend Anal. Chem.*, 39 (2012) 87.
9. Y. Wang, Z. Li, D. Hu, C. Lin, J. Li and Y. Lin, *J. Am. Chem. Soc.*, 132(2010) 9274.
10. Y. Wang, Z. Li , J. Wang, J. Li and Y. Lin, *Trends in Biotechnol.*, 29 (2011) 205.
11. L. Tang , Y. Wang, Y. Li, H. Feng, J. Lu and J. Li, *Adv. Funct. Mater.*, 19 (2009) 2782.
12. M. Zhou, Y. Zhai and S. Dong , *Anal. Chem.*, 81 (2009) 5603.
13. Y. Shao , J. Wang, H. Wu, J. Liu, I. A. Aksay and Y. Lin, *Electroanal.*, 22 (2010) 1027.

14. T. Kuila, S. Bose, P. Khanra, A. K. Mishra, N. H. Kim and J. H. Lee, *Biosens. Bioelectron.*, 26 (2011) 4637.
15. Z. Zhu , L. G. Gancedo , A. J. Flewitt, H. Xie, F. Moussy and W. I. Milne, *Sensors*, 12 (2012) 5996.
16. K. R. Ratinac, W. R. Yang, J. J. Gooding, P. Thordarson and F. Braet, *Electroanal.*, 23 (2011) 803.
17. L. Tang , H. Chang , Y. Liu and J. Li, *Adv. Funct. Mater.*, 24 (2012) 3083.
18. Y. Zhang, C. Zhang, W. Wang, X. Du, W. Dong, B. Han and Q. Chen, *J. Mater. Sci.*, 51 (2016) 6497.
19. S. Li, J Du, J. Zhang, M. Zhang and J. Chen, *Microchim Acta.*, 181 (2014) 631.
20. T. Tian, , L. Wang , F. Luan and X. Zhuang, *Talanta* 191 (2019) 103.
21. W. Wang, Y. Xie, C. Xia, H. Du and F. Tian, *Microchim. Acta.*, 181 (2014) 1325.
22. Y. Zhang, G. Zeng, L. Tang, J. Chen, Y. Zhu, X. He and Y. He, *Anal. Chem.*, 87 (2015) 989.
23. K. Szori, R. Puskas, G. Szollosi, I. Bertoti, J. Szepvolgyi and M. Bartok, *Catal. Lett.*, 143 (2013) 539.
24. G. Wang, J. Yang, J. Park, X. Gou, B. Wang, H. Liu and J. Yao, *J. Phys. Chem. C.*, 112 (2008) 8192.
25. D. F. Ba´ez, F. Tapia, P. Sierra-Rosales and S. Bollo, *Electroanalysis*, 30 (2018) 1.
26. M. Zhang, A. Smith and W. Gorski, *Anal. Chem.*, 76 (2004) 5045.
27. L. Zhu, R. Yang, X. Jiang and D. Yang, *Electrochem. Commun.*, 11 (2009) 530.
28. H. Hamidi, B. Haghghi, *Mater. Sci. Eng. C.*, 62 (2016) 423.
29. H. Chang, X. Wu, C. Wu, Y. Chen, H. Jiang and X. Wang, *Analyst*, 136 (2011) 2735.
30. X. Li, X. KanA, *Bioelectrochemistry*, 130 (2019) 107344.
31. M. B. Kamaç, E. K. Onat and M. Yılmaz, *Int J Anal Chem.*, 100(2020) 419.
32. X. Huang, J. Zhang, L. Zhang, H. Su, X. Liu, J. Liu, *Anal Biochem.*, 589(2020)113493.
33. S. Wang, Z. Yao, T. Yang, Q. Zhang, and F. Gao, *J Electrochem Soc.*, 166 (2019) G116.

© 2020 The Authors. Published by ESG (www.electrochemsci.org). This article is an open access article distributed under the terms and conditions of the Creative Commons Attribution license (<http://creativecommons.org/licenses/by/4.0/>).